ACS APPLIED MATERIALS & INTERFACES

Research Article

www.acsami.org

Biocompatible Ionic Liquid–Biopolymer Electrolyte-Enabled Thin and Compact Magnesium–Air Batteries

Xiaoteng Jia,[†] Yang Yang,[†] Caiyun Wang,*[,†] Chen Zhao,[†] R. Vijayaraghavan,[‡] Douglas R. MacFarlane,[‡] Maria Forsyth,[§] and Gordon G. Wallace*[,†]

[†]Intelligent Polymer Research Institute, ARC Centre of Excellence for Electromaterials Science, University of Wollongong, Wollongong 2522, Australia

[‡]School of Chemistry, ARC Centre of Excellence for Electromaterials Science, Monash University, Clayton, Victoria 3800, Australia

[§]Institute for Frontier Materials, ARC Centre of Excellence for Electromaterials Science, Deakin University, Burwood, Victoria 3125, Australia

ABSTRACT: With the surge of interest in miniaturized implanted medical devices (IMDs), implantable power sources with small dimensions and biocompatibility are in high demand. Implanted battery/supercapacitor devices are commonly packaged within a case that occupies a large volume, making miniaturization difficult. In this study, we demonstrate a polymer electrolyte-enabled biocompatible magnesium–air battery device with a total thickness of approximately 300 μm. It consists of a biocompatible polypyrrole–*para*(toluene sulfonic acid) cathode and a bioresorbable magnesium alloy anode. The biocompatible electrolyte used is made of choline nitrate (ionic liquid) embedded in a biopolymer, chitosan. This polymer electrolyte is mechanically robust and offers a high ionic conductivity of 8.9×10^{-3} S cm^{-1}. The assembled battery delivers a maximum volumetric power density of 3.9 W L^{-1}, which is sufficient to drive some types of IMDs, such as cardiac pacemakers or biomonitoring systems. This miniaturized, biocompatible magnesium–air battery may pave the way to a future generation of implantable power sources.

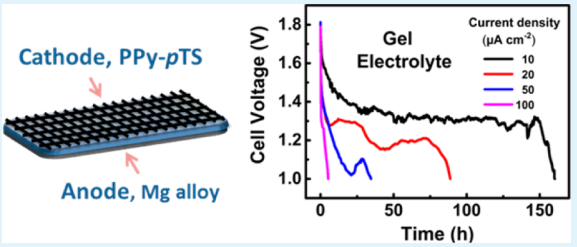

KEYWORDS: *polypyrrole, Mg–air batteries, biocompatible ionic liquid, chitosan, integrated solid-state batteries*

1. INTRODUCTION

Implanted medical devices (IMDs) including pacemakers,[1] microstimulators,[2] drug delivery microchips,[3] and others are impacting medical science. Power sources to drive IMDs are designed to meet strict clinical dimension constraints;[4] however, miniaturization of IMDs remains a challenge, that is hampered by battery size. Batteries normally account for a large volume of the overall IMD device and are typically constructed with a strong case encapsulating toxic/harmful chemicals to prevent their contact with the body.[5,6] Batteries could be more easily miniaturized if all of the components were biocompatible and integrated into one single, continuous unit without the need for packaging. Such an approach also allows the device to be fabricated in a thin-film manner with increased mechanical flexibility.[7]

Bioimplantable power sources built with biocompatible or biodegradable materials are of growing interest for future IMDs. These systems may have the ability to physically dissolve away after a period of stable operation if they employ bioresorbable metals or biodegradable polymers as electrodes. Rogers and co-workers recently reported a fully biodegradable Mg–Mo primary battery,[8] which demonstrated a discharge current of 100 μA cm^{-2} for 24 h in phosphate buffered saline (PBS) solution. This battery utilized biodegradable polyanhydride as a packaging material. Bettinger and co-workers developed an edible sodium-ion battery[9] with biologically derived melanin electrodes.[10] Potentials up to 0.6 V and currents in the range of 5–20 μA can be generated. Another recent advance in this field employs gastric juices in the digestive tract and a Zn anode in combination with a Pd cathode for powering a wireless endoscopy capsule.[11] They have also demonstrated their utility as a transient implanted power supply. However, these biodegradable transient batteries normally suffer from relatively short lifetimes and low power densities under physiological conditions.

There remains a need to develop novel power sources that are capable of performing longer lifetime under physiological conditions.[12,13] Such implantable batteries would rely on oxygen in the internal body fluid to produce a voltage between the anode and the cathode. Magnesium or its alloys present an appealing anode material due to its elemental abundance, overall benign nature, high theoretical specific charge capacity (2.2 Ah g^{-1}), and considerably negative electrode potential (−2.3 V versus SHE).[14,15] The rapid corrosion (degradation) of pure magnesium in aqueous solution limits use as an anode. The use of Mg alloy, AZ31, can deliver much better discharge

Received: September 2, 2014
Accepted: November 7, 2014
Published: November 7, 2014

characteristics due to its greatly improved corrosion resistance after the incorporation of Al and Zn elements. Biocompatible polypyrrole (PPy) has been shown to have potential applications in biomedical implants[16] and has been demonstrated to be a promising cathode material for biobatteries.[17,18] A biocompatible liquid electrolyte was used in these studies. To date, we are not aware of any report using biocompatible polymer electrolytes for this application. The use of a polymer electrolyte enables the components to be integrated to form a thin, compact configuration that is easy to implant.

Hence, the main objective of the present study is to develop a biocompatible polymer electrolyte based on a biocompatible ionic liquid embedded in a host biopolymer, chitosan (CS). CS is a versatile, abundant, and naturally occurring cationic polyelectrolyte that has been extensively studied for pharmaceutical and biomedical applications.[19−21] Room-temperature ionic liquids (ILs) are promising electrolytes because they possess negligible vapor pressure, low flammability, high ionic conductivity, and high electrochemical stability.[22,23] Among a variety of ILs, choline-based ILs are considered to be promising, low-toxicity ILs for a variety of biomedical applications.[24−26] This is mostly due to the fact that choline (more correctly cholinium) is a naturally occurring cation that shows very low toxicity and can work as a cell signaling agent.[27,28] Choline salts have also been used recently in IL−gel systems for cancer therapy delivery.[29] Choline nitrate, [Ch][NO_3], was chosen in this work due to its low viscosity, high conductivity, and biocompatibility. CS hydrogels incorporated with choline chloride and choline dihydrogen phosphate have demonstrated their utility in biocompatible multiresponsive drug delivery systems.[30]

In this study, we also demonstrated a compact biobattery system with the use of this thin-film gel electrolyte, chitosan−choline nitrate. Bioresorbable Mg alloy and biocompatible polypyrrole−*para*(toluene sulfonic acid) served as anode and cathode, respectively. This gel electrolyte is mechanically robust and offers a high ionic conductivity. The battery system can generate an open-circuit voltage of 1.80 V and an output power of 3.9 W L^{-1}, which could be sufficient to drive low-power IMDs such as cardiac pacemakers or biomonitoring systems.

2. EXPERIMENTAL SECTION

2.1. Materials. Pyrrole, toluene-4-sulfonic (sodium salt), glacial acetic acid (99%), sodium hydroxide (97%), choline hydroxide (20 wt % in water), nitric acid (70%), phosphate buffered saline (PBS) tablet, and chitosan (CS, M_v 60−120 K, 85% deacetylated degree) were obtained from Sigma-Aldrich. Pyrrole was freshly distilled. All other chemicals were used as-supplied. The PBS solution was prepared by dissolving one PBS tablet in 200 mL of deionized water. Magnesium alloy (AZ31) sheet with the nominal mass composition 96% Mg, 3% Al, and 1% Zn was purchased from Goodfellow Metals, UK. It was polished with fine sandpaper and degreased with acetone prior to use. The 316 type stainless steel (SS) mesh was purchased from Hongye Stainless Steel Wire Cloth Co. Ltd..

Choline-based ionic liquids were generally made by the neutralization reaction of the corresponding acid with choline hydroxide as described in the literature.[31] The synthesis of choline nitrate ([Ch][NO_3]) typically involved a dropwise addition of nitric acid aqueous solution to choline hydroxide aqueous solution in an ice bath, and the contents were stirred for about 2 h at room temperature. Then, water was removed by distillation, the ionic liquid was dried under vacuum, and the yield was found to be 98%. The ionic liquid was characterized as follows: mp 29 °C; electrospray mass spectroscopy analysis, (cone ±25 V): CN; *m*/*z* (relative intensity, %): ES^+, 103.9 ($Me_3N^+CH_2CH_2OH$, 100); ES^-, 62.0 (NO_3^-, 100).

2.2. Fabrication and Characterization of Chitosan−Choline Nitrate (CS−[Ch][NO_3]) Thin-Film Electrolytes. This thin-film electrolyte was prepared by a simple casting method. CS was dissolved in an acidic solution (1% v/v glacial acetic acid) to a concentration of 2 wt % and stirred overnight until a clear solution was obtained, followed by adding choline nitrate ([Ch][NO_3]). The weight ratios of CS to [Ch][NO_3] used were 1:1, 1:5, and 1:9. The mixtures were stirred continuously for 4 h, cast onto a Teflon mold, and dried at room temperature for 2 days. The films formed were dipped into an aqueous 0.1 M NaOH solution to remove any remaining acetic acid and washed several times with deionized water. They were dried for 24 h at room temperature and peeled off of the substrate. Their thickness was in the range of 60−100 μm. They were cut into 10 × 10 mm^2 squares for testing.

The residual water content of these films were measured using thermogravimetric analyses (TGA). TGA was conducted by heating the samples from room temperature to 500 °C at a heating rate of 10 °C min^{-1} under N_2 using a Q500 TGA analyzer (TA Instruments, UK). Fourier-transform infrared spectra (FTIR) measurements were recorded with a Shimadzu AIM8000 spectrometer. The mechanical properties of thin films were evaluated using a Shimadzu EZ mechanical tester with a 500 N load at an elongation rate of 10 mm min^{-1}. The ionic conductivity of ionic liquid and thin-film electrolytes were determined with ac impedance using a Gamry EIS 3000 system in the frequency range of 100 kHz to 1 Hz. The gel sample or the ionic liquid-saturated filter paper was sandwiched between two stainless steel plates with a testing area of 1.5 cm^2. The ionic conductivity (S cm^{-1}) was estimated according to the following equation

$$\sigma = \frac{d}{RA} \tag{1}$$

where d is the thickness of the film (cm), R is the bulk resistance (Ω) obtained from the first intercept on the x axis of the impedance data in the complex plane, and A is the contact area (cm^2).

The ionic liquid component may potentially separate from the polymer electrolyte due to lack of long-term compatibility of the liquid component and the CS when it is directly exposed to air. As a result, the conductivity of electrolyte will decrease and affect the Mg−air battery performance. An IL-leaching test was carried out by leaving the film electrolyte in open air under ambient conditions. The liquid released from the film was absorbed with Kimwipes until a constant weight was reached, and it was monitored every 24 h. The ionic liquid loss was calculated according to the following equation

$$\text{IL loss (\%)} = \frac{W_I - W_L}{W_{IL}} \times 100\% \tag{2}$$

where W_I is the initial weight of film and W_L is the film weight during the leaching test. W_{IL} is the initial weight of IL in the film. The ionic conductivity change was also monitored, and its loss was calculated according to the following equation

$$\text{ionic conductivity loss (\%)} = \frac{\sigma_I - \sigma_L}{\sigma_I} \times 100\% \tag{3}$$

where σ_I is the initial conductivity of the electrolyte film and σ_L is the electrolyte film conductivity during the leaching test.

2.3. Electropolymerization and Electrocatalytic Properties of Polypyrrole Electrode. The polypyrrole−toluene-4-sulfonic (PPy−*p*TS) film was galvanostatically electrodeposited onto a stainless steel mesh following reported procedures.[32] Briefly, the electrodeposition was conducted at a constant current of 0.5 mA cm^{-2} for 30 min in a solution containing 0.1 M pyrrole monomer and 0.1 M *p*-toluene sulfonic acid sodium salt. The surface morphologies of PPy−*p*TS were investigated by FE-SEM (JEOL JSM-7500FA).

The effect of oxygen on the reduced polypyrrole electrode was investigated by monitoring the open-circuit potential of the PPy−*p*TS electrode in nitrogen-saturated, oxygen-saturated, air-saturated, and normal PBS solutions (no gas disturbance), similar to the work reported by Wu et al.[17] The PPy−*p*TS electrode was first reduced at −0.8 V (vs Ag/AgCl) for 10 min, followed by gas introduction, if

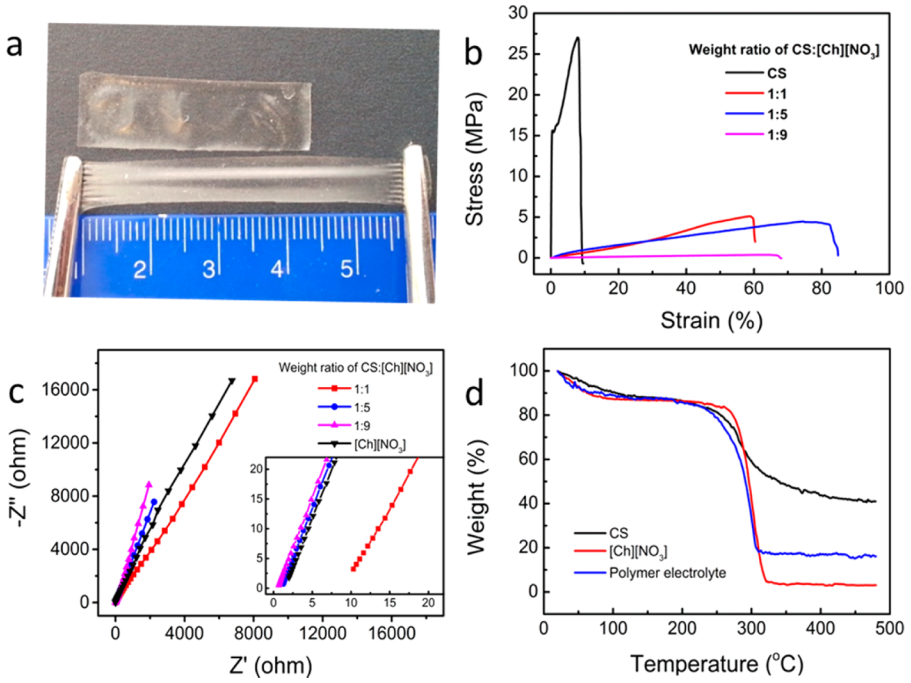

Figure 1. (a) Digital image of a CS−[Ch][NO_3] (1:5) polymer electrolyte film demonstrating its mechanical robustness; (b) stress−strain curves and (c) ac impedance spectra of polymer electrolyte films (inset, expanded view at high-frequency region); (d) TGA curves of chitosan film, ionic liquid, and CS−[Ch][NO_3] polymer electrolyte (1:5).

applied. The gas flow rate was controlled at 200 mL min^{-1}. Cyclic voltammetry of the PPy−*p*TS electrode was conducted in nitrogen- or oxygen-saturated PBS solution and was performed with an electrochemical workstation (CHI 650D) in a conventional three-electrode cell with a stainless steel mesh counter electrode and a Ag/AgCl (3 M NaCl) reference electrode.

2.4. Battery Assembly and Testing. The integrated solid-state battery was fabricated with a PPy film cathode (11 × 10 × 0.04 mm^3), Mg alloy anode (11 × 10 × 0.2 mm^3), and CS−[Ch][NO_3] polymer electrolyte film (10 × 10 × 0.06 mm^3). This electrolyte functioned as both electrolyte and separator. Two such electrodes with polymer electrolyte are pressed together face-to-face to form a sandwich structure. During the assembly process, a thin layer of CS−[Ch][NO_3] solution was dropped onto the electrode surface to hold all of the device components together like glue, improving the mechanical integrity. The tilted cross-sectional view (approximately 20°) of the solid-state battery was characterized using an optical microscope (Leica DM6000). We also assembled batteries with the same size electrodes in a one-component cell with 5 mL of PBS solution for comparison. The battery discharge tests were carried out by using a battery testing device (Neware Electronic Co., China). The cells were discharged galvanostatically to a cutoff cell voltage of 1.0 V. Electrochemical impedance spectra for cells were measured using a Gamry EIS 3000 system in the frequency range of 100 kHz to 0.01 Hz with an ac perturbation of 10 mV at open-circuit potential before and after discharge. Polarization curves of Mg alloy foils were obtained with the CHI workstation (CHI 650D) after being immersed in PBS solution and contacted with polymer electrolyte for 6 h under ambient conditions. They were performed at a scan rate of 1 mV s^{-1} using Mg alloy as the working electrode and a stainless steel mesh as the combined counter and reference electrodes.

3. RESULTS AND DISCUSSION

3.1. Characterization and Properties of CS−[Ch][NO_3] Polymer Electrolyte Film. Within the weight ratio range investigated, 1:1, 1:5, 1:9 (chitosan to [Ch][NO_3]), it was found that free-standing electrolyte films can be formed. These films are robust, and, for instance, the film formed at a ratio of 1:5 can withstand large mechanical deformation (Figure 1a).

The mechanical properties of these polymer electrolytes are shown in Figure 1b. The CS substrate exhibited a tensile strength of 27 MPa, being able to withstand a 32% elongation at break. When the weight ratio was 1:5 (CS/[Ch][NO_3]), the mechanical strength decreased to 4.5 MPa, and a 82% elongation at break was observed. After the introduction of [Ch][NO_3] into the CS matrix, the hydrogen-bonding interactions between polymer chains are reduced due to the plasticizing effect.[33] When the CS/[Ch][NO_3] ratio was 1:9, the mechanical strength was lowered to 0.4 MPa, and the elongation to break was slightly reduced to 66%. At higher choline nitrate content, film formation was not possible due to insufficient CS.

The pure CS film did not present any measurable ionic conductivity (<10^{-8} S cm^{-1}) (Figure 1c). Upon addition of [Ch][NO_3], the ionic conductivity was significantly enhanced to 7.3 × 10^{-4} S cm^{-1} when the weight ratio was 1:1 (CS/[Ch][NO_3]). This is attributed to the joint influence of the strong plasticizing effect of ionic liquid along with the inherent ionic conductivity introduced by the IL ions.[34] The ionic conductivity of a polymer electrolyte is related to the polymer chain motion, which increases with increasing plasticizer and continuously creates free volume into which the ions migrate.[35] With an increase in concentration of choline nitrate (ratio of 1:5), the conductivity increased to 6.2 × 10^{-3} S cm^{-1}, 1 order of magnitude higher than that of films with a ratio of 1:1. At a ratio of 1:9, the conductivity reached 8.9 × 10^{-3} S cm^{-1}. The limitation on the increase in conductivity with a large amount of IL may be related to the formation of ion aggregates, which decreased the number of effective charge carriers.[36] Interestingly, the ionic conductivity of CS−[Ch][NO_3] polymer electrolyte (1:5 and 1:9) is higher than that of pure ionic liquid [Ch][NO_3] (4.85 × 10^{-3} S cm^{-1}). This may be

Table 1. Basic Properties of CS−[Ch][NO_3] Polymer Electrolytes at Room Temperature

electrolyte sample (weight ratio)	resistance (ohm)	conductivity (S cm^{-1})	thickness (mm)	strength (MPa)	elongation at break (%)
CS	n/a		0.077	27.0	32
CS−[Ch][NO_3] (1:1)	10.31	7.3×10^{-4}	0.113	5.10	59
CS−[Ch][NO_3] (1:5)	1.279	6.2×10^{-3}	0.118	4.46	82
CS−[Ch][NO_3] (1:9)	0.896	8.9×10^{-3}	0.121	0.38	66

attributed to the increasing ionicity of the ionic liquid[37] induced by the presence of chitosan, which has highly polarizable substituents such as amino and hydroxyl groups. This phenomenon was also observed for chitosan-based gel electrolytes containing an imidazolium-based ionic liquid.[38]

The weight loss in TGA curves (Figure 1d) over the temperature range up to 150 °C was attributed to water vaporization. It was 9, 13, and 11% for the CS film, [Ch][NO_3], and CS−[Ch][NO_3] polymer electrolyte (1:5), respectively. The decomposition of the CS backbone occurred mainly at 230−350 °C due to the depolymerization of glucosamine units. The ionic liquid was stable up to 260 °C and decomposed at 320 °C. The CS−[Ch][NO_3] polymer electrolyte showed a similar thermal stability up to 230 °C as that of CS, followed by a sharp weight loss as that of IL, proving that its thermal stability was affected by these two components.

In this CS−[Ch][NO_3] gel polymer electrolyte system, the polymer CS provides mechanical support and dimensional stabilization, and the ionic liquid functions as a charge carrier and plasticizer for the polymer matrix. The mechanical and electrochemical properties of the polymer electrolyte are summarized in Table 1. CS−[Ch][NO_3] (1:5) polymer electrolyte film was selected for further tests due to its robust mechanical properties and high conductivity.

3.2. Electrocatalytic Properties of PPy−*p*TS Electrode. In a typical metal−air battery system, the oxygen reduction reaction (ORR) occurs at the cathode electrode/air electrode.[39] Noble metal Pt is a biocompatible electrocatalyst to ORR. However, the high cost limits its use. The PPy cathode would be reduced by the action of the electrochemical cell when coupled with Mg anode, and in the presence of oxygen, it would be reoxidized to create a catalytic cycle. To determine if the reduced PPy−*p*TS can be used as an ORR electrocatalyst, it was first reduced by applying a constant potential of −0.8 V for 10 min. The open-circuit potential of such reduced polypyrrole increased immediately after the applied current was removed (Figure 2a) due to the reoxidation of reduced polypyrrole. It is also noticed that a much higher potential increase can be produced with the introduction of an air or O_2 stream. A potential of 0.04, −0.03, and −0.27 V was measured after 10 min with O_2, air, and no gas bubbling, respectively. The high potential observed in the oxygen-rich solution demonstrates the effective reoxidation of reduced polypyrrole induced by oxygen reduction.

The ORR on PPy was also investigated using cyclic voltammetry in oxygen- or nitrogen-saturated PBS solution at a scan rate of 10 mV s^{-1} (Figure 2b). In N_2-saturated solution, the influence of oxygen could be excluded, and the redox peaks can be attributed to PPy only. In O_2-saturated solution, the cathodic peak became more pronounced, with a higher current response. The cathodic current increase can be attributed to the enhanced redox properties of polypyrrole in the presence of O_2. The reduced polypyrrole (close to the fully dedoped state) can be reoxidized by oxygen (and oxygen is reduced in that process). For the anodic peak, a slightly reduced current

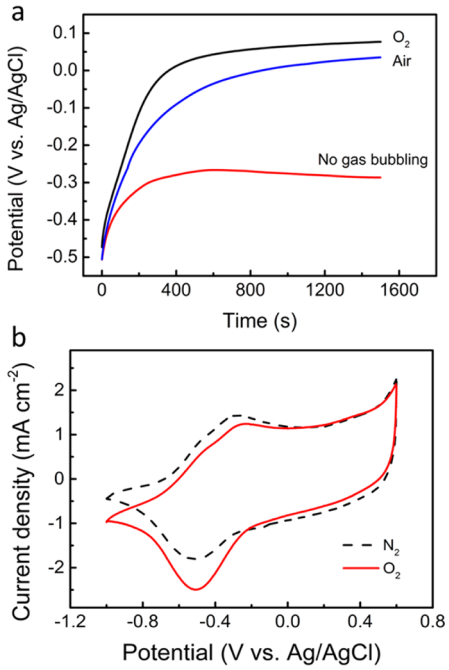

Figure 2. (a) Potential response of the reduced PPy−*p*TS electrode in PBS solution with O_2, air, or no gas bubbling after the applied potential (−0.8 V vs Ag/AgCl) was removed; (b) CV of a PPy−*p*TS electrode in N_2- or O_2-saturated PBS solution at a scan rate of 10 mV/s.

compared to that in N_2-saturated solution was observed. This can be attributed to less dedoped PPy available and concomitantly less electrons were involved in the electrochemical oxidation because some of them have been oxidized via oxygen molecules. This is consistent with previous reports.[40,41] It is believed that the carbon atoms on the pyrrole ring could supply an active site for oxygen chemical adsorption, which could weaken the O−O bond of oxygen and lower the activation energy for reduction according to the mechanism proposed by Khomenko et al.[42]

3.3. Battery Performance using CS−[Ch][NO_3] Polymer Electrolyte Film or PBS Solution Electrolyte. The integrated solid-state batteries are fabricated with the CS−[Ch][NO_3] film sandwiched between PPy−*p*TS cathode and Mg alloy anode, as shown schematically in Figure 3a. Thus, the polymer film functions both as the electrolyte and separator. During the assembly process, the gel polymer electrolyte could hold all of the device components together like a laminating adhesive, improving mechanical integrity. The PPy polymer (doped with toluene-4-sulfonic acid (*p*TS)) is grown on the stainless steel substrate using conditions described in the Experimental Section.

The discharge characteristics of cells at various current densities were investigated using a polymer electrolyte film and PBS solution electrolyte for comparison (Figure 4). The open-circuit voltages for the integrated solid-state batteries were in

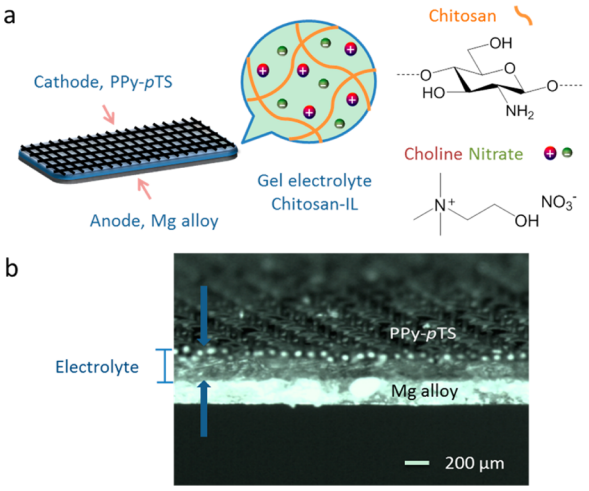

Figure 3. Schematic configuration (a) and optical image of cross-sectional view (20° tilted) (b) of the integrated solid-state Mg–air battery.

the range of 1.80–1.71 V just after the cell was assembled. The cell voltage dropped immediately when the discharge current was applied and soon reached a flat discharge plateau. At low current density, batteries using the film electrolyte delivered a slightly higher discharge plateau than that with PBS solution electrolyte. Specifically, at a current density of 10 μA cm^{-2}, the Mg|CS–[Ch][NO_3]|OH|O_2(aq)|PPy cell displayed a voltage of 1.33 V (middle point of the discharge curve) for up to 160 h, 40 mV higher than that of Mg|PBS|O_2(aq)|PPy cell (1.29 V). However, when the current density increased to 50 μA cm^{-2}, the Mg|CS–[Ch][NO_3]|OH|O_2(aq)|PPy cell could sustain a voltage of only 1.13 V for 35 h, 60 mV lower than that of Mg|PBS|O_2(aq)|PPy cell (1.19 V). The main cause for the lower discharge voltage of the solid-state battery at higher discharge current is likely due to the lower ion mobility in the polymer electrolyte. This creates a potential drop, the size of which depends on the resistivity of the electrolyte. To further support the hypothesis that this battery system involves processes involving Mg oxidation and O_2 reduction, a blank stainless steel (SS) mesh cathode was used as a control experiment. With a plain SS mesh as the cathode, this cell can be discharged for only 0.5 h to a cutoff voltage of 1.0 V (Figure 4a inset), in sharp contrast to that of 88.7 h using the PPy electrode at the same discharge current of 20 μA cm^{-2}. This supports the proposal that PPy plays a catalytic role in oxygen reduction. The contribution from the SS mesh is negligible. SS mesh acts as an underlying conductive substrate material for PPy electropolymerization and as a current collector in this work. After the discharge experiment, Mg alloy was treated in an ultrasonic

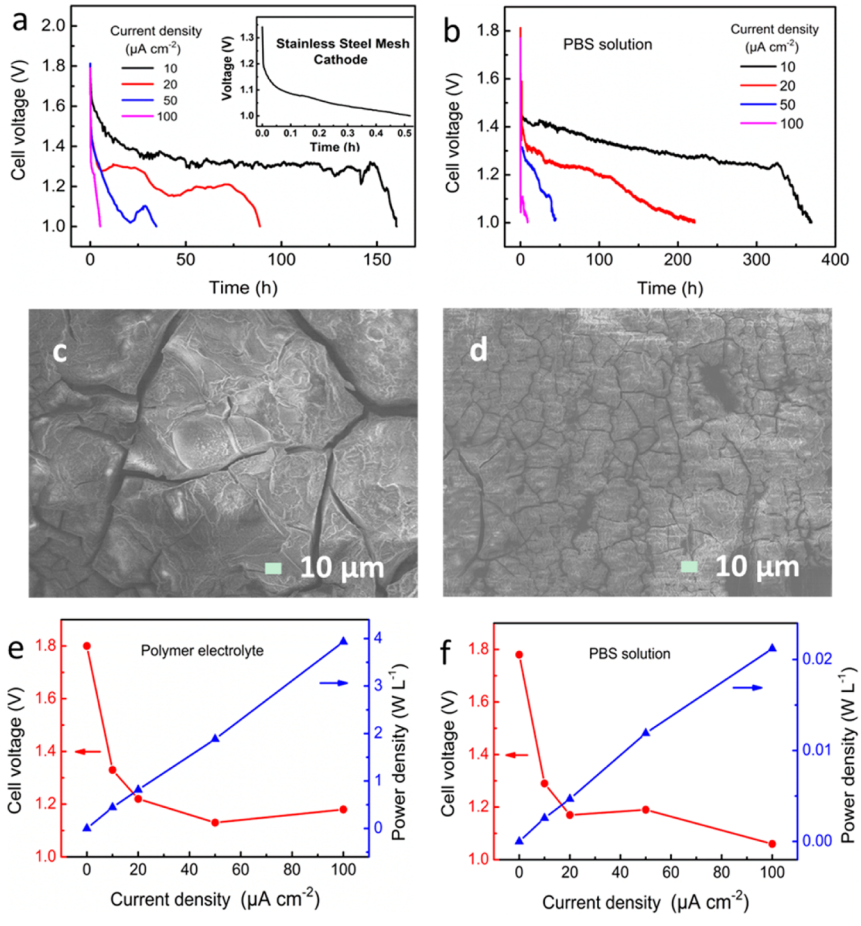

Figure 4. Discharge curves of Mg–air batteries with PPy cathode and Mg alloy anode at various discharge current densities using CS–[Ch][NO_3] (1:5) film electrolyte (a) and PBS solution electrolyte (b); SEM images of AZ31 surfaces after the discharge experiment at a current density of 20 μA cm^{-2} using CS–[Ch][NO_3] (1:5) film electrolyte (c) and PBS solution electrolyte (d); plateau voltage and the corresponding power density of Mg batteries as a function of discharge current densities using CS–[Ch][NO_3] (1:5) film (e) and PBS solution (f) as electrolyte. (inset to panel a: discharge curve of Mg–air battery using stainless steel mesh cathode as control.)

dx.doi.org/10.1021/am505985z | ACS Appl. Mater. Interfaces 2014, 6, 21110–21117

bath (H_2O) for 5 min, followed by rinsing with H_2O. A great number of cracks were formed on the Mg alloy electrode after use in PBS solution (Figure 4d). This is attributed to hydrogen evolution, as occurs on rapid oxidation of Mg.[43] In contrast, many fewer cracks were observed with the polymer electrolyte (Figure 4c), which may be explained by the reduced corrosion rate of magnesium alloy.

In order to evaluate the practical performance of the battery, we calculated the volumetric power density. The plateau voltages ranged between 1.33 and 1.13 V with an applied discharge current density in the range of 10−100 μA cm^{-2} (Figure 4e). Compared with the recently reported biodegradable Mg−Mo primary battery,[8] this novel battery structure exhibited a much higher voltage than that previously reported (0.4−0.7 V) and had a longer lifetime up to 160 h compared to 24 h. This battery system also delivered a maximum volumetric power density of 3.9 W L^{-1}, which is almost 200 times higher than that (0.02 W L^{-1}) from the same size electrode in 5 mL of PBS. This was attributed to the large dead volume when PBS electrolyte was used. Nevertheless, a maximum energy density of 72 Wh L^{-1} could be generated from this solid-state battery, much higher than that (2.2 Wh L^{-1}) of the flexible thin-film lithium-ion battery reported previously.[44] Generally, the power requirements of active IMDs fall in the level of micro- to milliwatts.[5] This integrated solid-state battery could thus become a power source for some IMDs, such as cardiac pacemakers or biomonitoring systems. A higher power output can be achieved using devices connected in series.

The electrochemical impedance spectra for both the solid-state and liquid electrolyte batteries were collected before and after 6 h of discharge (Figure 5). They exhibited similar Nyquist plots, with a compressed semicircle in the high to medium frequency range. This semicircle was associated with the charge transfer reaction at the electrolyte/electrode interface.[45] The charge transfer resistance, R_{ct}, was 1175 ohm with film electrolyte and 243 ohm in PBS. After the discharge (6 h), this R_{ct} of the cell with PBS electrolyte was 577 ohm, much lower than that of solid-state battery (3968 ohm). The large resistance of the solid-state battery can be mainly ascribed to a low ion migration rate in the polymer electrolyte. The low ion movement can decrease the ion exchange rate at the interface and consequently deteriorate the catalytic efficiency of the cathode. The greatly increased resistance of polymer electrolyte during discharge was the main cause for the lower discharge voltage of the solid-state battery at higher discharge current.

To determine the corrosion behavior of the Mg anode, its polarization behavior was investigated in these two electrolytes, with a stainless steel mesh serving as both the counter and reference electrodes (Figure 5c). Prior to the scan, the Mg anode was left at open-circuit potential in both electrolytes for 6 h until a steady, free corrosion potential value was recorded. The corrosion potential shifted toward more positive potential from −2.12 V using PBS solution to −1.72 V with the polymer electrolyte. The anodic and cathodic current densities decreased by nearly an order of magnitude. These results clearly demonstrated that the anodic dissolution of Mg was hindered by the use of polymer electrolyte, and a better discharge performance may be obtained. This may explain the higher discharge plateau obtained at low charge density (10 μA cm^{-2}) using the polymer electrolyte. However, the reduced ionic mobility also limited the battery performance at higher discharge current.

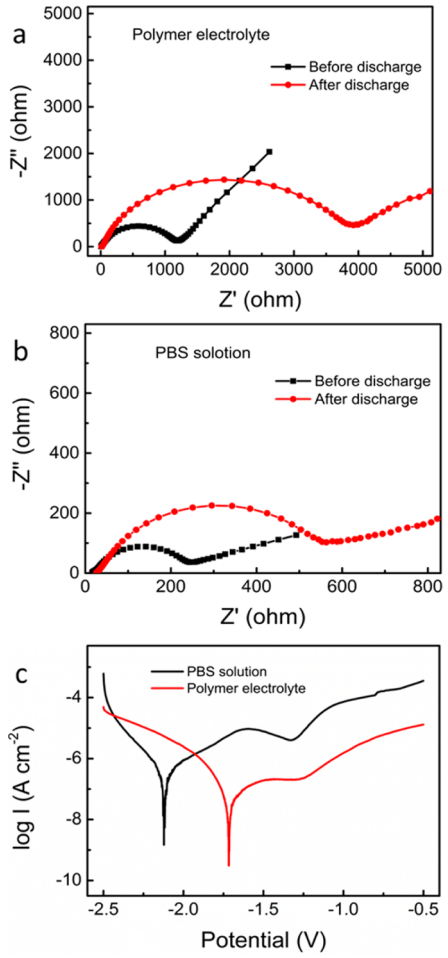

Figure 5. Electrochemical impedance spectra of Mg−air batteries before and after discharge at a current density of 20 μA cm^{-2} for 6 h using CS−[Ch][NO_3] (1:5) film (a) and PBS solution (b) as electrolytes; (c) polarization curves of Mg alloy |electrolytes|SS at a scan rate of 1 mV s^{-1}.

It has previously been reported that ionic liquid leakage from the polymer matrix reduces ionic conductivity.[46] To evaluate the IL retention ability in the polymer electrolyte film during long-term operation, an IL-leaching test was carried out by leaving the film electrolyte in open air under ambient conditions.

It was observed that liquid was expelled from the polymer matrix onto the polymer surface. Such liquid exhibited the same characteristic peaks in the FTIR spectra as that of [Ch][NO_3] (Figure 6a), indicating that the released liquid is the IL ([Ch][NO_3]) or an aqueous solution of it. The percentage of IL leached from the film electrolyte during 1 week is shown in Figure 6b. It can be seen that the film weight remained nearly steady after a 120 h testing period. The weight loss was 13.4% after 168 h. The IL leakage from the film reflects the fact that the IL is not anchored to the polymer chain via strong hydrogen bonds and can easily partition into a IL−water phase on the surface. The ionic conductivity decreased to 4.9 × 10^{-3} S cm^{-1} (21.5% loss) after 168 h (Figure 6b). This conductivity is still high enough to maintain battery operation.

4. CONCLUSIONS

The results presented in this work indicate a promising approach to the fabrication of miniaturized biocompatible

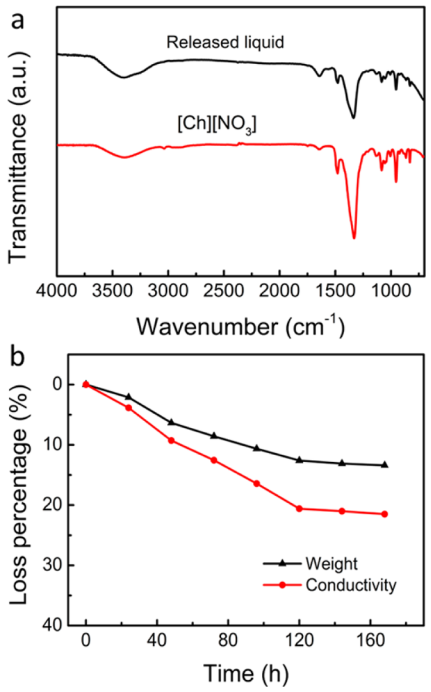

Figure 6. (a) FTIR spectrum of the released liquid from CS–[Ch][NO_3] (1:5) film electrolyte and pure ionic liquid [Ch][NO_3]; (b) weight loss (%) and ionic conductivities change of the film electrolyte during the IL-leaching test under ambient conditions.

batteries employing a bioresorbable metal anode, biocompatible conducting polymer cathode, and biocompatible polymer electrolyte. This polymer electrolyte functions as an electrolyte, separator, and as the glue to hold all of the device components together. With a whole device volume of 30 mm^3, the integrated solid-state battery can generate an open-circuit voltage of 1.80 V and a maximum output power of 118 μW, which could be sufficient to drive some low-power IMDs such as cardiac pacemakers or biomonitoring systems. In contrast to conventional aqueous biobatteries, this integrated solid-state battery would occupy minimal space. However, its performance declines at higher discharge currents due to the low ion mobilities. Given its small device dimensions and biocompatibility, this battery may be a promising power source for miniaturized implantable medical devices. Despite our battery system using the biocompatible cathode, bioresorbable anode, and biocompatible electrolyte, a conformal biocompatible O_2-permeable and proton-transporting encapsulation layer[8] is recommended for practical applications to prevent direct contact with body tissues and also to provide a barrier to any peroxide products.

AUTHOR INFORMATION

Corresponding Authors

*Tel: +61 2 42981426. Fax: +61 2 42983114. E-mail: caiyun@uow.edu.au (C.W.).

*Tel: +61 2 42213127. Fax: +61 242213124. E-mail: gwallace@uow.edu.au (G.G.W.).

Notes

The authors declare no competing financial interest.

ACKNOWLEDGMENTS

The authors thank the Australia Research Council (ARC) for financial support. The authors also acknowledge the use of facilities within the Australian National Fabrication Facility (ANFF) Materials Node and the UOW Electron Microscopy Centre. G.G.W., M.F., and D.R.M. are grateful to the ARC for support under the Australian Laureate Fellowship scheme.

REFERENCES

(1) Southcott, M.; MacVittie, K.; Halamek, J.; Halamkova, L.; Jemison, W. D.; Lobel, R.; Katz, E. A Pacemaker Powered by an Implantable Biofuel Cell Operating under Conditions Mimicking the Human Blood Circulatory System—Battery not Included. *Phys. Chem. Chem. Phys.* **2013**, *15*, 6278–6283.

(2) Chung, A. J.; Huh, Y. S.; Erickson, D. A Robust, Electrochemically Driven Microwell Drug Delivery System for Controlled Vasopressin Release. *Biomed. Microdevices* **2009**, *11*, 861–867.

(3) Elman, N. M.; Duc, H. L. H.; Cima, M. J. An Implantable MEMS Drug Delivery Device for Rapid Delivery in Ambulatory Emergency Care. *Biomed. Microdev.* **2009**, *11*, 1387–2176.

(4) Muskovich, M.; Bettinger, C. J. Biomaterials-Based Electronics: Polymers and Interfaces for Biology and Medicine. *Adv. Healthcare Mater.* **2012**, *1*, 248–266.

(5) Wei, X.; Liu, J. Power Sources and Electrical Recharging Strategies for Implantable Medical Devices. *Front. Energy Power Eng. China* **2008**, *2*, 1–13.

(6) Kong, Y.; Wang, C.; Yang, Y.; Too, C. O.; Wallace, G. G. A Battery Composed of a Polypyrrole Cathode and a Magnesium Alloy Anode—toward a Bioelectric Battery. *Synth. Met.* **2012**, *162*, 584–589.

(7) Heller, A. Potentially Implantable Miniature Batteries. *Anal. Bioanal. Chem.* **2006**, *385*, 469–473.

(8) Yin, L.; Huang, X.; Xu, H.; Zhang, Y.; Lam, J.; Cheng, J.; Rogers, J. A. Materials, Designs, and Operational Characteristics for Fully Biodegradable Primary Batteries. *Adv. Mater.* **2014**, *26*, 3879–3884.

(9) Kim, Y. J.; Chun, S.; Whitacre, J. F.; Bettinger, C. J. Self-Deployable Current Sources Fabricated from Edible Materials. *J. Mater. Chem. B* **2013**, *1*, 3781–3788.

(10) Kim, Y. J.; Wu, W.; Chun, S.; Whitacre, J. F.; Bettinger, C. J. Biologically Derived Melanin Electrodes in Aqueous Sodium-Ion Energy Storage Devices. *Proc. Natl. Acad. Sci. U.S.A.* **2013**, *110*, 20912–20197.

(11) Mostafalu, P.; Sonkusale, S. Flexible and Transparent Gastric Battery: Energy Harvesting from Gastric Acid for Wireless Endoscopy Applications. *Biosens. Bioelectron.* **2014**, *54*, 292–296.

(12) Bock, D. C.; Marschilok, A. C.; Takeuchi, K. J.; Takeuchi, E. S. Batteries Used To Power Implantable Biomedical Devices. *Electrochim. Acta* **2012**, *84*, 155–164.

(13) Wang, S.; Lin, L.; Wang, Z. L. Nanoscale Triboelectric-Effect-Enabled Energy Conversion for Sustainably Powering Portable Electronics. *Nano Lett.* **2012**, *12*, 6339–6346.

(14) Rahman, M. A.; Wang, X.; Wen, C. High Energy Density Metal–Air Batteries: A Review. *J. Electrochem. Soc.* **2013**, *160*, A1759–A1771.

(15) Cheng, F.; Chen, J. Metal–Air Batteries: From Oxygen Reduction Electrochemistry to Cathode Catalysts. *Chem. Soc. Rev.* **2012**, *41*, 2172–2192.

(16) George, P. M.; Lyckman, A. W.; LaVan, D. A.; Hegde, A.; Leung, Y.; Avasare, R.; Testa, C.; Alexander, P. M.; Langer, R.; Sur, M. Fabrication and Biocompatibility of Polypyrrole Implants Suitable for Neural Prosthetics. *Biomaterials* **2005**, *26*, 3511–3519.

(17) Wu, A.; Venancio, E. C.; MacDiarmid, A. G. Polyaniline and Polypyrrole Oxygen Reversible Electrodes. *Synth. Met.* **2007**, *157*, 303–310.

(18) Wang, C.; Zheng, W.; Yue, Z.; Too, C. O.; Wallace, G. G. Buckled, Stretchable Polypyrrole Electrodes for Battery Applications. *Adv. Mater.* **2011**, *23*, 3580–3584.

(19) Bhattarai, N.; Gunn, J.; Zhang, M. Chitosan-Based Hydrogels for Controlled, Localized Drug Delivery. *Adv. Drug Delivery Rev.* **2010**, *62*, 83–99.

(20) Croiser, F.; Jerome, C. Chitosan-Based Biomaterials for Tissue Engineering. *Eur. Polym. J.* **2013**, *49*, 780–792.

(21) Kumar, M. N.; Muzzarelli, R. A. A.; Muzzarelli, C.; Sashiwa, H.; Domb, A. J. Chitosan Chemistry and Pharmaceutical Perspectives. *Chem. Rev.* **2004**, *104*, 6017−6084.
(22) Opallo, M.; Lesniewski, A. A Review on Electrodes Modified with Ionic Liquids. *J. Electroanal. Chem.* **2011**, *656*, 2−16.
(23) Smiglak, M.; Pringle, J. M.; Lu, X.; Han, L.; Zhang, S.; Gao, H.; MacFarlane, D. R.; Rogers, R. D. Ionic Liquids for Energy, Materials, and Medicine. *Chem. Commun.* **2014**, *50*, 9228−9250.
(24) Curto, V. F.; Scheuermann, S.; Owens, R. M.; Vijayaraghavan, R.; MacFarlane, D. R.; Benito-Lopez, F.; Diamond, D. Probing the Specific Ion Effects of Biocompatible Hydrated Choline Ionic Liquids on Lactate Oxidase Biofunctionality in Sensor Applications. *Phys. Chem. Chem. Phys.* **2014**, *16*, 1841−1849.
(25) Fukaya, Y.; Iizuka, Y.; Sekikawa, K.; Ohno, H. Bio Ionic Liquids: Room Temperature Ionic Liquids Composed Wholly of Biomaterials. *Green Chem.* **2007**, *9*, 1155−1157.
(26) Weaver, K. D.; Kim, H. J.; Sun, J. Z.; MacFarlane, D. R.; Elliott, G. D. Cyto-Toxicity and Biocompatibility of a Family of Choline Phosphate Ionic Liquids Designed for Pharmaceutical Applications. *Green Chem.* **2010**, *12*, 507−513.
(27) Brock, M.; Nickel, A. C.; Madziar, B.; Blusztajn, J. K.; Berse, B. Differential Regulation of the High Affinity Choline Transporter and the Cholinergic Locus by cAMP Signaling Pathways. *Brain Res.* **2007**, *1145*, 1−10.
(28) Vijayaraghavan, R.; Thompson, B. C.; MacFarlane, D. R.; Kumar, R.; Surianarayanan, M.; Aishwarya, S.; Sehgal, P. K. Biocompatibility of Choline Salts as Crosslinking Agents for Collagen Based Biomaterials. *Chem. Commun.* **2010**, *46*, 294−296.
(29) Kumar, S. S. D.; Surianarayanan, M.; Vijayaraghavan, R.; Mandal, A. B.; MacFarlane, D. R. Curcumin Loaded Poly(2-hydroxyethyl methacrylate) Nanoparticles from Gelled Ionic Liquid—in Vitro Cytotoxicity and Anti-cancer Activity in Skov-3 Cells. *Eur. J. Pharm. Sci.* **2014**, *51*, 34−44.
(30) Dias, A. M. A.; Cortez, A. R.; Barsan, M. M.; Santos, J. B.; Brett, C. M. A.; Sousa, H. C. Development of Greener Multi-Responsive Chitosan Biomaterials Doped with Biocompatible Ammonium Ionic Liquids. *ACS Sustainable Chem. Eng.* **2013**, *1*, 1480−1492.
(31) Winther-Jensen, O.; Vijayaraghavan, R.; Sun, J.; Winther-Jensen, B.; MacFarlane, D. R. Self Polymerising Ionic Liquid Gel. *Chem. Commun.* **2009**, 3041−3043.
(32) Zhao, C.; Wang, C.; Yue, Z.; Shu, K.; Wallace, G. G. Intrinsically Stretchable Supercapacitors Composed of Polypyrrole Electrodes and Highly Stretchable Gel Electrolyte. *ACS Appl. Mater. Interfaces* **2013**, *5*, 9008−9014.
(33) Yoshida, C. M. P.; Oliveira, E. N.; Franco, T. T. Chitosan Tailor-Made Films: The Effects of Additives on Barrier and Mechanical Properties. *Packag. Technol. Sci.* **2009**, *22*, 161−170.
(34) Sekhon, S. S.; Krishnan, P.; Singh, B.; Yamada, K.; Kim, C. S. Proton Conducting Membrane Containing Room Temperature Ionic Liquid. *Electrochim. Acta* **2006**, *52*, 1639−1644.
(35) Sakurai, K.; Maegawa, T.; Takahashi, T. Glass Transition Temperature of Chitosan and Miscibility of Chitosan/Poly(*N*-vinyl pyrrolidone) Blends. *Polymer* **2000**, *41*, 7051−7056.
(36) Reece, D. A.; Ralph, S. F.; Wallace, G. G. Metal Transport Studies on Inherently Conducting Polymer Membranes Containing Cyclodextrin Dopants. *J. Membr. Sci.* **2005**, *249*, 9−20.
(37) Ueno, K.; Tokuda, H.; Watanabe, M. Ionicity in Ionic Liquids: Correlation with Ionic Structure and Physicochemical Properties. *Phys. Chem. Chem. Phys.* **2010**, *12*, 1649−1658.
(38) Yamagata, M.; Soeda, K.; Ikebe, S.; Yamazaki, S.; Ishikawa, M. Chitosan-Based Gel Electrolyte Containing an Ionic Liquid for High-Performance Nonaqueous Supercapacitors. *Electrochim. Acta* **2013**, *100*, 275−280.
(39) Lee, J. S.; Kim, S. T.; Cao, R. G.; Choi, N. S.; Liu, M.; Lee, K. T.; Cho, J. Metal−Air Batteries with High Energy Density: Li−Air versus Zn−Air. *Adv. Energy Mater.* **2011**, *1*, 34−50.
(40) Jiang, C. M.; Lin, X. Q. A Novel Nanocomposite of Pd Nanocluster/Poly(*N*-acetylaniline) Nanorod Modified Electrode for the Electrocatalytic Reduction of Oxygen. *J. Appl. Electrochem.* **2008**, *38*, 1659−1664.
(41) Liu, H. Y.; Zhang, G. Q.; Zhou, Y. F.; Gao, M. M.; Yang, F. L. One-Step Potentiodynamic Synthesis of Poly(1,5-diaminoanthraquinone)/Reduced Graphene Oxide Nanohybrid with Improved Electrocatalytic Activity. *J. Mater. Chem. A* **2013**, *1*, 13902−13913.
(42) Khomenko, V. G.; Barsukov, V. Z.; Katashinskii, A. S. The Catalytic Activity of Conducting Polymers toward Oxygen Reduction. *Electrochim. Acta* **2005**, *50*, 1675−1683.
(43) Song, G. L. Control of Biodegradation of Biocompatible Magnesium Alloys. *Corros. Sci.* **2007**, *49*, 1696−1701.
(44) Koo, M.; Park, K.; Lee, S. H.; Suh, M.; Jeon, D. Y.; Choi, J. W.; Kang, K.; Lee, K. J. Bendable Inorganic Thin-Film Battery for Fully Flexible Electronic Systems. *Nano Lett.* **2012**, *12*, 4810−4816.
(45) *Electrochemical Impedance: Analysis and Interpretation*; Scully, J. R., Silverman, D. C., Kendig, M. W., Eds.; ASTM International: Philadelphia, PA, 1993.
(46) Rahman, M.; Brazel, C. S. The Plasticizer Market: An Assessment of Traditional Plasticizers and Research Trends To Meet New Challenges. *Prog. Polym. Sci.* **2004**, *29*, 1223−1248.